This article was downloaded by:
On: *25 January 2011*
Access details: *Access Details: Free Access*
Publisher *Taylor & Francis*
Informa Ltd Registered in England and Wales Registered Number: 1072954 Registered office: Mortimer House, 37-41 Mortimer Street, London W1T 3JH, UK

Liquid Crystals
Publication details, including instructions for authors and subscription information:
http://www.informaworld.com/smpp/title~content=t713926090

An investigation of the porosity and surface roughness of liquid crystal alignment layers using neutron reflectivity

P. L. Phillips; R. M. Richardson; A. Zarbakhsh; S. D. Haslam

Online publication date: 29 June 2010

To cite this Article Phillips, P. L. , Richardson, R. M. , Zarbakhsh, A. and Haslam, S. D.(1997) 'An investigation of the porosity and surface roughness of liquid crystal alignment layers using neutron reflectivity', Liquid Crystals, 23: 5, 699 — 708

To link to this Article: DOI: 10.1080/026782997207975

URL: http://dx.doi.org/10.1080/026782997207975

PLEASE SCROLL DOWN FOR ARTICLE

Full terms and conditions of use: http://www.informaworld.com/terms-and-conditions-of-access.pdf

This article may be used for research, teaching and private study purposes. Any substantial or systematic reproduction, re-distribution, re-selling, loan or sub-licensing, systematic supply or distribution in any form to anyone is expressly forbidden.

The publisher does not give any warranty express or implied or make any representation that the contents will be complete or accurate or up to date. The accuracy of any instructions, formulae and drug doses should be independently verified with primary sources. The publisher shall not be liable for any loss, actions, claims, proceedings, demand or costs or damages whatsoever or howsoever caused arising directly or indirectly in connection with or arising out of the use of this material.

LIQUID CRYSTALS, 1997, VOL. 23, NO. 5, 699–708

An investigation of the porosity and surface roughness of liquid crystal alignment layers using neutron reflectivity

by P. L. PHILLIPS, R. M. RICHARDSON*, A. ZARBAKHSH†
School of Chemistry, University of Bristol, Cantock's Close, Bristol BS8 1TS, U.K.

and S. D. HASLAM
D.R.A., St. Andrews Road, Malvern, Worcs WR14 3PS, U.K.

(*Received 17 March 1997; in final form 29 May 1997; accepted 23 June 1997*)

Neutron reflectivity has been used to investigate the porosity and surface roughness of three different liquid crystal alignment layers to elucidate how they orient the director. The absorption of hexane into these alignment layers was measured by neutron reflection and the volume fraction profile of the hexane within the layers was determined using the contrast variation method. Measurements were made on rubbed polyimide and silicon monoxide (SiO) evaporated at 5° and 30° to the substrate. The porosity and surface roughness of the alignment layers were found to be correlated with the induced pre-tilt of the director. The low pre-tilt rubbed polyimide and SiO 30° alignment layers were found to be smooth, uniform and impervious to hexane, whilst the high pre-tilt SiO 5° was porous and extremely rough. These observations suggest that both polyimide and SiO 30° rely on an anisotropic interaction with the surface rather than one induced by the surface topography. In contrast, the alignment of liquid crystals by SiO 5° probably originates from an interaction between the mesogens and the rough, porous surface.

Downloaded At: 20:19 25 January 2011

1. Introduction

In the past two decades, the technology required for the development of liquid crystal (LC) displays has made great progress. In these devices, a liquid crystal is sandwiched between two glass plates which are usually 2–10 μm apart. The undersides of the glass are treated with conducting indium tin oxide and then with an alignment layer which constrains the molecules to lie approximately parallel to the cell surface. Since it is the uniaxiality of the liquid crystal which is the prerequisite for good optical performance, any directional deviations of the optic axis within the cell would degrade the contrast between the light and dark states. Thus we recognize the crucial role of alignment layers in the operation of these devices. To date, several methods of liquid crystal alignment have been explored. The most commonly used are rubbed polymers [1], in particular polyimide, and obliquely evaporated silicon monoxide, SiO [2]. Despite the success of these methods, the mechanisms for liquid crystal alignment by these two layers are still unclear and as will be shown, may be quite different.

* Author for correspondence.
† Present address: Department of Chemistry, Science Laboratories, University of Durham, South Road, Durham DH1 3LE, U.K.

It was Berreman [3] who first attributed the origin of liquid crystal alignment to the elastic interaction between the liquid crystal and the micro-grooves introduced onto the substrate by rubbing. This provided a feasible alignment mechanism for glass rubbed with diamond dust. Indeed micro-grooves have been observed in the rubbing direction of rubbed polyimide films. Atomic force microscopy, AFM [4, 5] and scanning electron microscopy, SEM [6] studies have assessed their size and density. Several features were observed, e.g. numerous scratches mostly less than 1 nm deep, surface islands, point defects and a general modified background texture indicating that all the surface had been contacted during rubbing. From X-ray scattering measurements, it was found that the polymer strands were orientated in the rubbing direction and that the LC director lay within 20° of this axis [7].

Despite the proven existence of the micro-grooves, there is much evidence to suggest that alignment by rubbed polyimide is brought about by some other mechanism. In particular, Pidduck *et al*. [5] applied the Berreman theory of alignment to the scratches/micro-grooves they observed on rubbed polyimide samples during AFM measurements. They found the calculated anchoring energy to be far lower than the one observed experimentally; thus the topographic features could not

0267–8292/97 $12·00 © 1997 Taylor & Francis Ltd.

solely be responsible for the azimuthal anchoring of the director. Also, Ishihara *et al.* [8] observed alignment perpendicular to the rubbing direction on films of polystyrene. Subsequently, they proposed that it was the directional interaction along the side phenyl groups that was responsible for alignment and not the micro-grooves. Also, Geary *et al.* [9] showed that smectic alignment could be achieved from straight chain crystalline polymers in the absence of rubbing and micro-grooves. They then proposed that LC alignment by rubbed polyimide results from the favourable interactions between liquid crystal molecules and the polymer chains which became elongated when rubbed.

The case is even less clear for SiO alignment layers. Up to now, two mechanisms for their LC aligning properties have been discussed. The first of these involves order electricity, whereby a macroscopic electric polarization is induced when the symmetry of the phase is broken by the SiO [10]. The second mechanism concerns the topographical features of the SiO. Using the columnar model of Goodman–van der Waterbeemd, it has been suggested that the LCs could reside in the pillar vicinity, thus becoming influenced by the pillar orientation [11].

Downloaded At: 20:19 25 January 2011

In view of the importance of porosity in the latter mechanism or process, we have investigated the porosity of these layers further. Although Matsui *et al.* have already observed the uptake of various compounds into the pillar-like structure of high pre-tilt SiO [12], no depth dependence of the absorption was established. In this paper, we have studied the depth dependence of the porosity of both SiO and rubbed polyimide with the object of clarifying their mechanisms for LC alignment in more detail. Using the specular reflection of neutrons, the penetration of hexane into these alignment layers was monitored and the volume fraction profile of the solvent determined. The surface structure of the alignment layers was also elucidated.

Liquid crystals were not used in this experiment as they are extremely expensive to obtain in deuteriated form. Also, their structure would complicate the data obtained by introducing intense peaks into the reflectivity profiles [13]. This would lead to the weaker features in the data being obscured and the vital alignment layer interface information would be lost. Since 5–10 membered alkyl chains form a constituent part of many liquid crystals, the absorption of hexane into alignment layers should be similar to many liquid crystal materials although it will not provide direct information on the influence of the surface on the director or layer orientation in a mesophase. However we believe the experiment provides detailed surface structural information which gives valuable insight into the behaviour of liquid crystals at similar interfaces.

Three alignment layers were studied: rubbed polyimide and SiO evaporated at 5° (SiO 5°) and 30° (SiO 30°) to the surface. The two different SiO layers were studied because they induce high and low pre-tilts [14] (typically 30–40° for SiO 5° and 0° for SiO 30°), which often influence the eventual LC structure formed within the device. Thus, despite their similar composition, their interactions with the surfacial mesogens are obviously quite different. By examining their surface roughness and porosity, we might explain this phenomenon since the nature of the interface should play a key role in determining the eventual orientation of the director. For example, a rough surface may induce a high pre-tilt if the liquid crystals intermix with the surface protrusions and become forced to lie at an angle to the surface. By comparing the SiO results with those obtained from the polyimide, Probimide-32 (Ciba-Geigy), which is known to induce a low pre-tilt (typically 2–3°), we might establish a correlation between porosity/surface roughness and pre-tilt.

Care is required when using the term 'high' and 'low' pre-tilt. Essentially, pre-tilts are measured using optical phase retardation techniques on the bulk of a nematic liquid crystal. As pointed out by Barmentlo *et al.* [15] using second harmonic generation (SHG) measurements, this overall bulk pre-tilt can originate from quite different configurations of the surfacial mesogens. In particular, when rubbed polyimides were investigated with the cyanobiphenyl, 8CB, the zero bulk pre-tilt condition corresponded to a set of tilted molecules at the surface whose orientations were symmetrically distributed parallel and antiparallel to the rubbing direction. This symmetric tilt then relaxed after a few molecular widths from the surface to produce a bulk phase composed of mesogens aligned parallel to the cell surface.

Thus when we use the term 'low pre-tilt', we are simply referring to this absence of substantial preference of alignment parallel or antiparallel to the rubbing direction. Whether or not the surfacial molecules lie parallel or tilted with respect to the surface is not clear for the low pre-tilt polyimide and SiO 30° alignment layers used in this experiment.

2. Neutron reflection

The technique of the specular reflection of neutrons gives information on the refractive index profile normal to an interface. The refractive index, μ, is closely related to the scattering power of the constituent elements; hence, neutron reflection can provide information about the composition of surfaces. The refractive index is given by

$$\mu = 1 - \frac{\lambda^2 \rho}{2\pi} \quad (1)$$

where λ is the wavelength of the neutrons and ρ is the scattering length density of the medium. ρ is the product of the coherent scattering lengths, b_i, of the constituent

elements, i, and their respective number densities, n_i, i.e.

$$\rho = \sum_i n_i b_i. \quad (2)$$

Unlike X-rays, neutrons are scattered by nuclei, not electrons, so b can vary dramatically between isotopes of the same element. An important example is that of H and D ($b_H = 3{\cdot}741 \times 10^{-5}$ Å, $b_D = 6{\cdot}671 \times 10^{-5}$ Å). This was exploited in this work to vary the scattering length density of the hexane solution by changing the ratio of hexane and d_{14}-hexane.

Specular reflectivity is measured as a function of $\mathbf{Q}$, the scattering vector perpendicular to the surface. The magnitude of $\mathbf{Q}$ depends upon the grazing angle of incidence, θ, and the wavelength, λ, of the neutron

$$|Q| = \frac{4\pi}{\lambda} \sin\theta. \quad (3)$$

From Snells law, we find that there is a critical value of $\mathbf{Q} = \mathbf{Q}_c \equiv 4(\pi\rho)^{1/2}$ below which all the incident beam is totally externally reflected and there is no transmission into the sample.

Downloaded At: 20:19 25 January 2011

The specular reflectivity from a surface is well described by the kinematic approximation [16] at $\mathbf{Q} \gg \mathbf{Q}_c$. The reflectivity, $R(Q)$, of a neutron beam reflected from a surface is given by

$$R(Q) = R_F(Q)|\phi(Q)|^2 \quad (4)$$

where R_F is the theoretical Fresnel decay [17] that describes the reflectivity observed from an ideal smooth interface and ϕ is the film factor containing the surface structural information. In fact ϕ is simply the Fourier transform of the gradient of the scattering length density (SLD) profile, i.e.

$$\phi(Q) = \frac{1}{\Delta\rho} \int_{-\infty}^{\infty} \frac{\partial\rho(z)}{\partial z} \exp(iQz)\,dz \quad (5)$$

where $\Delta\rho$ is the difference in scattering length density of the two semi-infinite media either side of the interface.

This approach allows the reflectivity to be described in terms of partial structure factors [18]. For the system studied in this work, the scattering length density can be expressed

$$\rho(z) = b_{Si} n_{Si}(z) + b_{SiO} n_{SiO}(z) + b_{hex} n_{hex}(z) \quad (6)$$

where b_i is the scattering length of species i and n_i is its number density. We can then write the expression for the reflectivity as

$$R(Q) = \frac{16\pi^2}{\mathbf{Q}^4}(b_{SiO}^2 h_{SiOSiO}^{(1)} + b_{hex}^2 h_{hexhex}^{(1)} + b_{Si}^2 h_{SiSi}^{(1)} + 2b_{SiO} b_{hex} h_{SiOhex}^{(1)} + 2b_{SiO} b_{Si} h_{SiOSi}^{(1)} + 2b_{Si} b_{hex} h_{Sihex}^{(1)}) \quad (7)$$

where $h^{(1)}$ is the partial structure factor of species i and is correlated to the number density of this species by

$$h_{ij}^{(1)}(Q) = \mathrm{Re}(n_i^{(1)}(Q) n_j^{(1)*}(Q)), \qquad h_{ii}^{(1)}(Q) = |n_i^{(1)}(Q)|^2 \quad (8)$$

and

$$n_i^{(1)}(Q) = \int_{-\infty}^{\infty} \frac{\partial n_i(z)}{\partial z} \exp(iQz)\,dz. \quad (9)$$

If three measurements, $R_1(Q)$, $R_2(Q)$ and $R_3(Q)$, are made using different values of the mean scattering length of the hexane molecules (i.e. b_1, b_2 and b_3), it is possible to directly obtain the hexane partial structure factor. This can be derived from the second difference of three measurements

$$h_{hexane} = \left(\frac{\Delta R_{12}}{b_1 - b_2} - \frac{\Delta R_{13}}{b_1 - b_3}\right) \frac{\mathbf{Q}^4}{16\pi^2(b_2 - b_3)} \quad (10)$$

where $\Delta R_{12}(Q) = R_1(Q) - R_2(Q)$, etc. This shows that in principle, the partial structure factor can be determined from the reflectivity measurements without assuming a model scattering length density profile.

It is important to stress that such a determination is usually possible by combining reflectivity measurements with different isotopic labelling. It is generally not possible to make a unique surface structure determination from a single measurement. For instance, in the kinematic approximation, the two scattering length density profiles shown in figure 1 below would give identical reflectivities. Therefore analysis of such reflection data would be liable to give the wrong model.

However, despite the simplicity of this second difference method described above, we did not adopt it because of the difficulties in making corrections for small discrepancies between the nominal values of the hexane average scattering length and those suggested by the experimental results. These small inconsistencies arose from hexane evaporation that occurred when the mixed deuteriated and hydrogenous solutions were prepared.

The method that was used to determine the surface structure was to assume a volume fraction profile, $\psi(z)$, for the alignment layer material and then calculate the scattering length density profile beyond the silicon substrate using the formula

$$\rho(z) = \rho_L^0 \psi(z) + \rho_H^0 [1 - \psi(z)] \quad (11)$$

where ρ_L^0 and ρ_H^0 are the scattering length densities of the pure alignment layer and hexane phases, respectively. The value of ρ_H^0 would depend on the isotopic composition of the liquid.

The volume fraction profile was modelled by a number of slabs of thickness d_j, volume fraction ψ_j and with an interslab roughness of u_j. The reflectivity was then

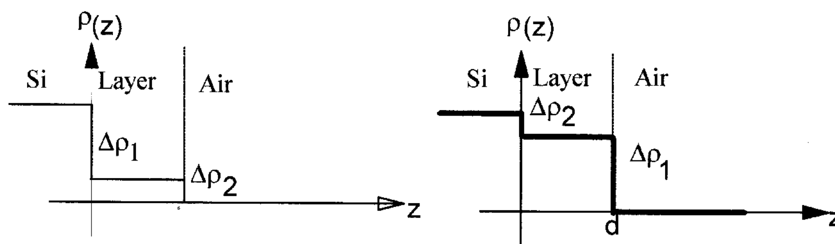

Figure 1. An example of scattering length density profiles that would give identical reflectivity data in the kinematic approximation.

calculated for each value of ρ_{H}^{0} using the optical matrix method [19] which is exact using the construction due to Abeles [20]. The parameters in this model were then adjusted simultaneously to fit the reflectivity data from the samples with different isotopic contents of hexane. As discussed above, the partial structure factor of hexane is defined by three reflection measurements on the sample with three mean scattering lengths for the hexane. It follows that if we can simultaneously fit an appropriate model structure [defined by equation (11)] to each of those three data sets, then the model must have the correct hexane structure (i.e. volume fraction profile). Any features of the scattering length density profile other than those associated with the hexane (such as inhomogeneities within the alignment layer) would also be correct and perhaps would have otherwise remained unresolved using the partial structure factor method.

Downloaded At: 20:19 25 January 2011

3. Experimental

3.1. *Preparation of alignment layers*†

3.1.1. *Rubbed polyimide*

A 10% solution of the polyimide–polyamide mixture PI-32 (Ciba-Geigy, Germany) in *N*-methylpyrrolidone was spin coated onto a polished silicon, Si(1 1 1) substrate at 3000 rpm for 30 s. The sample was then baked to remove excess solvent and rubbed unidirectionally using a Buehler rayon cloth attached to a rotating roller [21].

3.1.2. *Obliquely evaporated silicon monoxide (SiO)*

The SiO alignment layers were prepared by oblique evaporation of SiO onto the Si(1 1 1) surface [11]. The SiO flux made an angle of 85° or 60° to the substrate normal for the high and low pre-tilt alignment layers, respectively.

3.2. *Sample environment*

The following sample holder (figure 2) was designed to hold the silicon block with the alignment layer completely immersed in a trough of hexane. Owing to

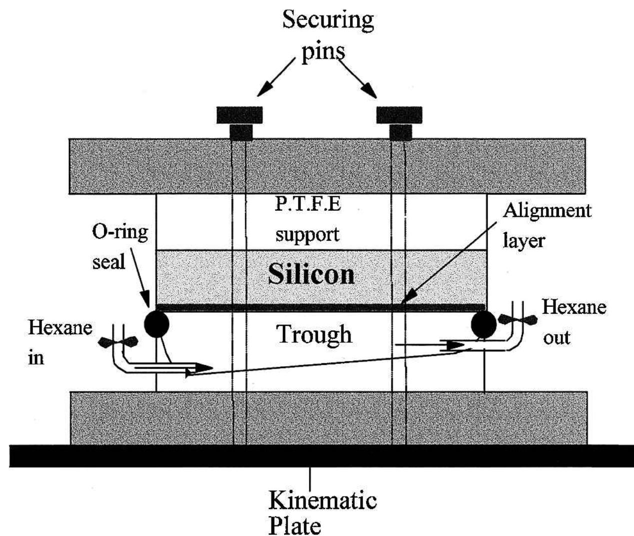

Figure 2. The solid/liquid cell.

the high transparency of silicon to neutrons, the block was inverted so that silicon formed the incident medium. The trough was designed with a sloping base to facilitate the expulsion of air bubbles from the cell when filled from the lower tap.

For each layer, a measurement was initially made with the trough empty to establish the SLD profile of the alignment layers when dry. Measurements were then made for each alignment layer with the four different scattering length densities of hexane as shown in table 1. The four different percentage deuteriations were chosen to highlight different features within the sample. For example, the 43% hexane solution contrast matched the silicon and thus highlighted the features within the

Table 1. Percentage deuteriation and corresponding scattering length densities of the hexane solutions used.

Percentage (by volume) of deuteriation of hexane	Nominal scattering length density/Å^{-2}
100	$6{\cdot}14\times10^{-6}$
68	$4{\cdot}0\times10^{-6}$
43	$2{\cdot}1\times10^{-6}$
0	$-0{\cdot}58\times10^{-6}$

†All alignment layer coatings were prepared at the Defence Research Agency, St. Andrews Road, Malvern, Worcs WR14 3PS, U.K.

alignment layer, whilst the 100% deuteriated solution gave a strong solvent signal. After the acquisition of a full data set, the cell was completely drained of hexane before the next solution was introduced into the cell. The first surplus drops of hexane to emerge from the cell when refilled with the next solution were discarded to limit any cross-contamination between measurements.

3.3. *Data acquisition*

The reflectivity data were collected using the white beam time of flight method at the ISIS pulsed neutron source, Rutherford Appleton Laboratory, U.K. Using the CRISP [22] reflectometer for the polyimide and SiO 5° samples, and the SURF [23] reflectometer for the SiO 30° samples, measurements were made at angles of incidence of 0·25°, 0·6° and 1·5° with an angular resolution ($\Delta\theta/\theta$) of the order of 6% for all samples. The wavelength band was defined by a single disc chopper enabling measurements to be made over a **Q**-range of 0·008–0·6 Å^{-1}. The intensity of the reflected beam was recorded using a detector and the absolute reflectivity was calculated by normalizing the detector spectrum to the monitor spectrum.

Downloaded At: 20:19 25 January 2011

3.4. *Data reduction*

The three data sets obtained for each sample were individually scaled to overlap so that they formed a single profile. Usually, reflectivity data are scaled by equating the intensity of the total external reflection region to unity. However, owing to the absence of a critical edge in some of the data, an alternative method had to be adopted. Scaling is usually necessary due to the different efficiencies of the detector and monitor. However, for high reflectivity, there is a possibility that detector saturation can occur at short wavelengths, so it was not possible to scale the data by simply dividing by a spectrum from the incident beam falling directly onto the detector. First the wavelength dependence of the transmission of the silicon block was measured by placing it between two low efficiency monitors to avoid saturation. All subsequent reflectivity data were then corrected for this factor. The absolute scale factor for the lowest angle run was then determined from the high wavelength limit of the spectrum from the same beam falling directly on the detector.

3.5. *Data analysis*

For each sample studied, a model volume fraction profile was assumed. This was later converted into a SLD profile using the individual scattering length densities of the hexane solutions and an educated guess at the alignment layer scattering length density. Using the optical matrix method, a model reflectivity profile was then calculated for each hexane contrast. Using a least squares analysis fitting routine, the data were simultaneously fitted to their corresponding data sets such that the eventual choice of volume fraction profile would then be the one that produced the best fit for *all* contrasts. This ensured a unique result and avoided the possibility of a rogue solution that could arise if the different contrasts were fitted individually.

Parameters such as layer thickness, volume fraction, and surface roughness were all variable, whilst incident medium and hexane SLDs, background and resolution parameters all remained fixed. The following treatment of surface roughness was adopted. Since long range undulations affect the final reflectivity in the same way as the beam divergence might, this can be incorporated into the model fit by use of an increased beam divergence parameter. The local short range undulations, on the other hand, need a more subtle treatment. Their main contributing factor to the reflectivity is the removal of intensity from the specular direction. The exact treatment of this is complex [24], but to a good approximation, we can assume the surface roughness to affect the resulting reflectivity in a similar fashion to that of a diffuse interface. Thus the treatment of this roughness follows the method proposed by Névot and Crocé [25]. This method consists of applying a Gaussian type factor to the Fresnel reflectivity coefficient for each interface between layers, i.e.

$$r_{ij}(Q) = r_{ij}^{\text{ideal}}(Q)\,\exp\left(-\frac{1}{2}Q_i Q_j u^2\right) \qquad (12)$$

where r_{ij} is the Fresnel reflection coefficient for the interface between layers i and j, Q_i and Q_j are related to the angle of the beam in these layers and u is the second moment of the line dividing the two slabs if the interface is rough.

4. Results and discussion

The reflectivity data (points), model fits (solid lines) and corresponding volume fraction profiles are presented in figures 3–8. Some of the data sets have been uniformly shifted from their original position for clarity. The results obtained from each will now be discussed individually.

4.1. *Rubbed polyimide*

The reflectivity data for the rubbed polyimide sample consisted of a uniform set of interference fringes superimposed onto a Fresnel decay curve. The large amplitude of the fringes resulted from sharp interfaces present within the sample, and the good SLD contrasts between the Si, polyimide and hexane. The uniform fringes are associated with the interference observed from a *single* layer SLD profile. Thus, an appropriate single layer model SLD profile was assumed and subsequent parameter refinement yielded a layer thickness of 211 ± 5 Å

Downloaded At: 20:19 25 January 2011

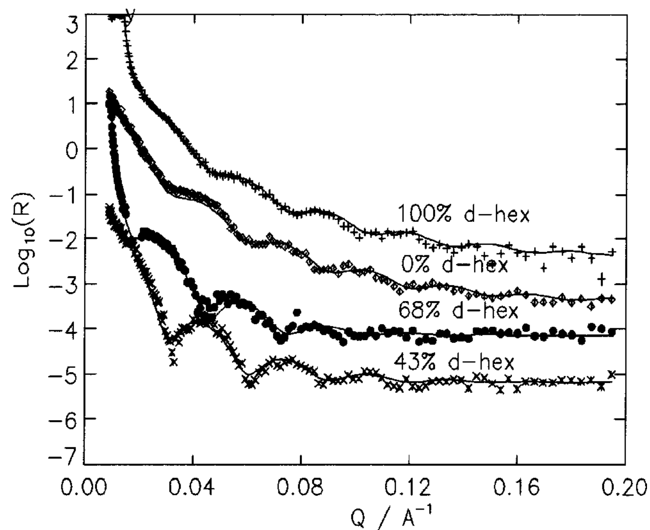

Figure 3. Reflectivity from Si/polyimide/hexane. The 100% data have been shifted by 3, the 0% data by 2 and the 68% by 1 for clarity.

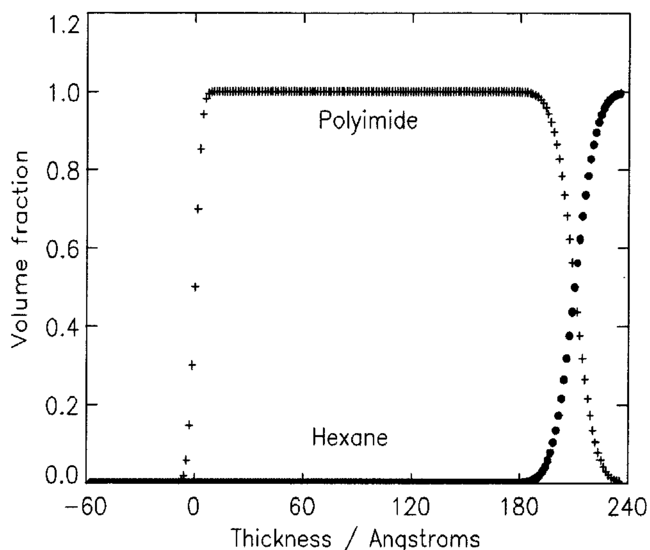

Figure 4. Polyimide/hexane volume fraction profiles.

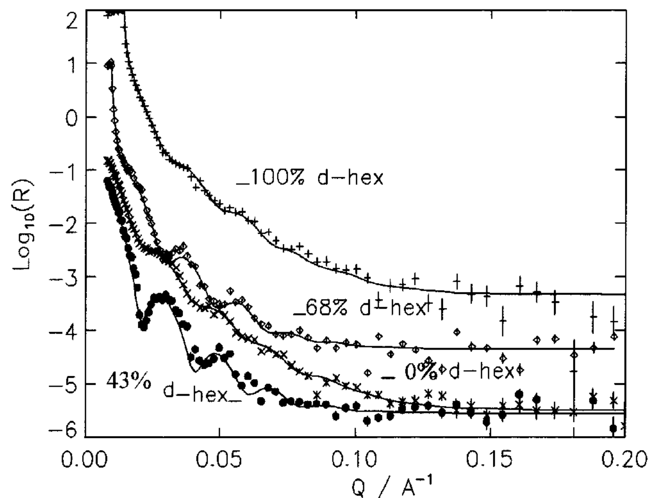

Figure 5. Reflectivity from Si/SiO 30°/hexane. The 100% data have been shifted by 2 and the 68% by 1 for clarity.

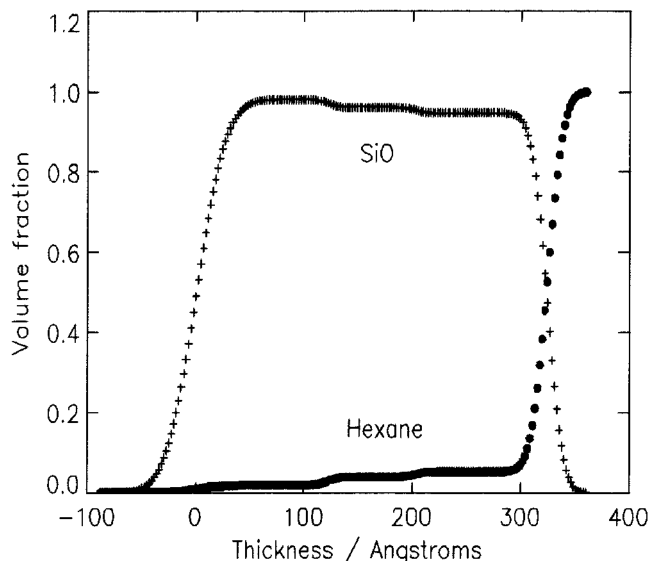

Figure 6. SiO 30°/hexane volume fraction profiles.

and corresponding SLD of $(2{\cdot}7 \pm 0{\cdot}1) \times 10^{-6}\,\text{Å}^{-2}$. The values are typical of such layers and correspond well with those from the dry sample. Both surface and interfacial roughnesses were found to be between 3 and 5 Å which are also typical of rubbed polyimides [7]. In particular, Haslam and Pidduck observed a root-mean-square roughness of 3 Å for Probimide-32 using AFM techniques [26].

From the volume fraction profile, it is evident that no hexane penetrated the polyimide. The absence of any notable surface roughness or mixed solvent/polyimide layers indicates that surface micro-grooves (often observed to be several manometers deep [27]) were absent. However, AFM measurements have shown that although the surface of rubbed Probimide-32 is essentially flat and featureless, small grooves of various sizes and sparsely distributed large grooves (few nm deep and fractions of a micron wide) are indeed present [7]. In view of this positive identification of the grooves, we conclude that they must be distributed very sparsely about the polymer surface such that the layer appears essentially smooth and impervious.

The size difference between the hexane chains and liquid crystal molecules enhances the unlikeliness of any polymer–mesogen intermixing within devices utilizing these alignment layers. Also, no cross-contamination or adsorbed layers of hexane solutions were observed. We therefore conclude that an anisotropic interaction

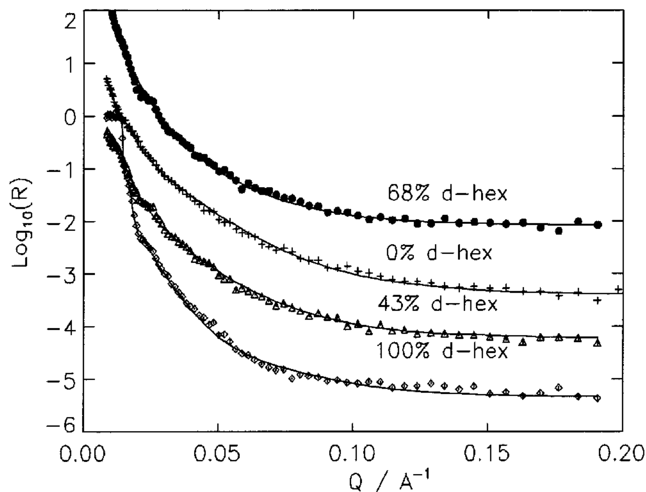

Figure 7. Reflectivity from Si/SiO 5°/hexane. The 68% data have been shifted by 3, the 0% data by 2 and the 43% by 1 for clarity.

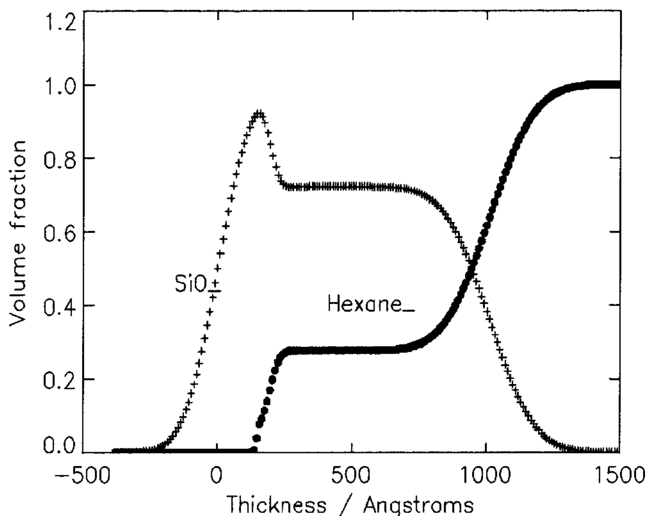

Figure 8. SiO 5°/hexane volume fraction profiles.

Downloaded At: 20:19 25 January 2011

between the polymer chains and interfacial mesogens is responsible for alignment.

4.2. *SiO* 30°

The reflectivity data obtained from the SiO 30° sample were similar to those obtained from the polyimide. A single uniform layer model SLD profile provided a good fit to the data; however a small amount of hexane absorption had to be involved to fit the data. The layer was found to be 322 ± 5 Å thick with a scattering length density of $(2{\cdot}6 \pm 0{\cdot}2) \times 10^{-6}$ Å^{-2} and a surface roughness of around 16 Å. Again, these values corresponded well with the data obtained from the layer in the dry sample.

As seen from the volume fraction profile, the absorption increased slightly at the surface, but the layer was never found to contain more than 5% (by volume) hexane. It should be noted that the discrete layers displayed in the volume fraction profile are probably not real. They are a simplistic representation of a smoothly varying volume fraction profile generated by the fitting routine.

Since the volume fraction of hexane in the SiO is small (and that of the larger liquid crystal molecules would probably be less) it seems unlikely that the alignment mechanism relies on these absorbed molecules. Owing to the fractal nature of these surfaces [28] and the absence of any reported directional dependence of the surface topography, it is difficult to put forward any other steric mechanisms for alignment. This is further complicated by the fact that as previously reported by Uchida *et al.* [11] and Jerome *et al.* [29], an antisymmetric planar alignment is realized by use of these layers. That is, the molecules lie with an azimuthal angle perpendicular to that of the pillar tilt, with their long axes approximately parallel to the cell surface. Also, glancing angle neutron diffraction measurements made on SiO 30° have shown that the pillar tilt with respect to the surface normal is small ($<5°$) and that the pillars themselves are poorly defined [30]. Thus, a topographical description of alignment by these layers seems to be inadequate and further work is required to clarify the associated mesogen–SiO interactions.

4.3. *SiO* 5°

The results from this alignment layer were rather different. In contrast to the other samples, the data were somewhat featureless and completely inconsistent with the single layer model. The absence of any fringes in the data meant that the exact functional form of the hexane volume fraction profile could not be isolated since several models, although very similar, gave equally good fits to the data. Thus, the simplest of these models was adopted to give an insight into the degree of porosity rather than the exact depth dependence of the absorption.

The scattering length density profile of the SiO layer in the absence of any hexane was found to be non-uniform. An approximately 150 Å thick low density ($\rho = 2{\cdot}8 \times 10^{-7}$ Å^{-2}) layer was found at the SiO–Si interface which could have resulted from the sparse distribution of the nucleation sites formed during the evaporation process. The scattering length density of the layer then rose to $2{\cdot}3 \pm 0{\cdot}3 \times 10^{-6}$ Å^{-2} for the remaining 810 ± 30 Å of SiO. The surface roughness was found to be in excess of 100 Å which is consistent with AFM measurements [28] and was probably a major contributor to the absence of interference fringes in much of the data.

From the SiO and hexane volume fraction profiles (obtained from the SiO in the presence of hexane), it is clear that this layer was substantially porous to hexane.

The upper 800 Å contained almost 30% by volume of hexane which over a distance of approximately 200 Å, gradually increased to 100% in the bulk liquid. This has major implications for the alignment mechanism as the possibility of liquid crystal penetration into the SiO is now certain. The high porosity suggests that liquid crystal molecules are likely to reside between the pillars which in turn, could influence the orientation and tilt of the mesogens [11].

It also seems likely that coupled with the surface roughness, the induced tilt could be a major contributing factor to the origin of the molecular pre-tilt since this phenomenon was not encountered in the other two low/zero pre-tilt layers. Also, recent glancing angle neutron diffraction measurements on SSFLCs using these alignment layers have confirmed that the molecular long axes lie in the direction approximately parallel to the pillar tilt direction [31]. If the surfacial mesogens reside between the pillars, the observed pre-tilt could then simply be a manifestation of the pillar tilt on the mesogens, whereby the symmetry of the distribution of the surface tilts is removed.

The parameters used to fit all the data from the three samples are summarized in tables 2 and 3. The volume fractions quoted are those of the alignment layers and the roughnesses u_{ij} are those between layers i and j.

5. Individuality of the model fits

Steps were taken to ensure that the model hexane volume fraction profiles obtained from the fitting process were unique. For example, a correlation between layer scattering length density and volume fraction is often encountered when fitting a single reflectivity profile. Although the contrast variation technique and the simultaneous fitting of the data should keep this uncertainty minimal, it is still important to be aware of multiple solutions. To assess the correlation between the alignment layer SLD and volume fraction, a range of values of each was selected and fixed. The fitting routine was then executed for all combinations of these fixed values, recording the goodness of fit, chi, (χ), squared, for each case. For every execution of the routine, a fixed number of iterations was performed such that the parameters had reached their optimum values before the next cycle. Plots of χ^2 vs layer SLD and volume fraction are displayed for each of the three samples in figures 9–11 below.

As can be seen for the polyimide and SiO 30°, a single minimum in χ^2 was located in the position of the previously quoted optimum values for layer SLD and volume fraction. The absence of any correlation between the two parameters is conveyed by the sharpness of the minimum; thus the solution obtained was unique. It

Downloaded At: 20:19 25 January 2011

Table 2. Parameters obtained from the model fits to the experimental data.

Parameter	Polyimide	SiO 30°	SiO 5°
SLD of pure alignment layer/Å^{-2}	$2{\cdot}7 \pm 0{\cdot}1 \times 10^{-6}$	$2{\cdot}6 \pm 0{\cdot}2 \times 10^{-6}$	$2{\cdot}3 \pm 0{\cdot}3 \times 10^{-6}$
Beam divergence/°	0·03 ± 0·003	0·03 ± 0·003	0·03 ± 0·003
Surface roughness/Å	4 ± 1	7 ± 2	98 ± 8
Thickness layer 1/Å	211 ± 5	133 ± 2	146
Volume fraction 1	1·0	0·99 ± 0·01	1·0
Roughness, u_{12}/Å	—	8 ± 2	5 ± 1
Thickness layer 2/Å	—	70 ± 2	40 ± 3
Volume fraction 2	—	0·98 ± 0·01	1·0
Roughness, u_{23}/Å	—	8 ± 2	40 ± 5
Thickness layer 3/Å	—	110 ± 2	811 ± 20
Volume fraction 3	—	0·95 ± 0·01	0·72 ± 9·8
Substrate roughness/Å	4 ± 1	7 ± 2	176 ± 10

Table 3. Nominal and experimental scattering length densities of the hexane solutions used in the experiments.

Percentage of d-hexane	Nominal SLD/10^{-6} Å^{-2}	Experimentally determined SLD/10^{-6} Å^{-2}		
		Polyimide	SiO 30°	SiO 5°
100%	6·14	6·14 ± 0·005	6·14 ± 0·005	6·14 ± 0·005
68%	3·99	3·72 ± 0·05	4·02 ± 0·08	3·73 ± 0·05
43%	2·31	1·9 ± 0·05	1·64 ± 0·05	1·60 ± 0·05
0%	−0·58	−0·58 ± 0·005	−0·58 ± 0·005	−0·58 ± 0·005

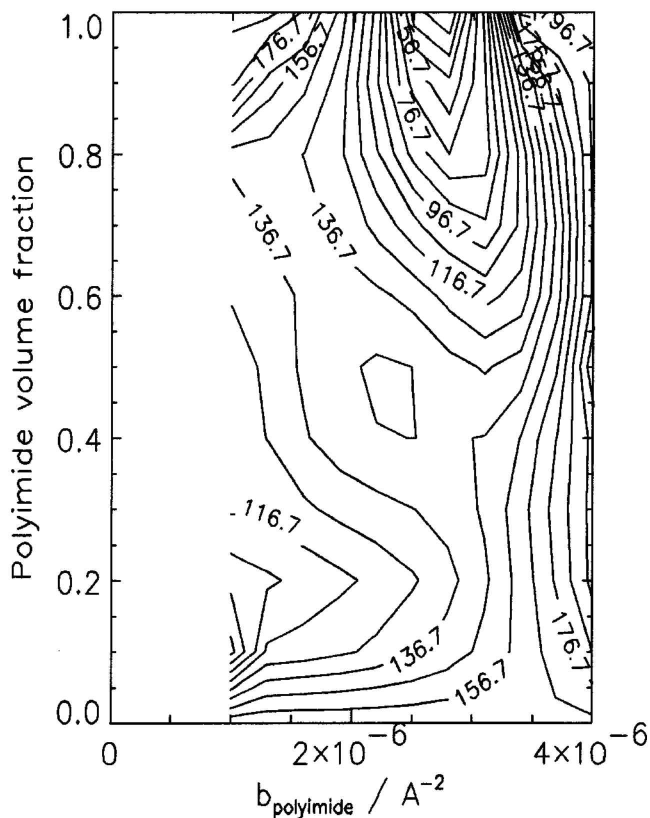

Figure 9. Contour χ^2 plot to show minimum at ($2{\cdot}7 \times 10^{-6}$ Å^{-2}, 1) for rubbed polyimide.

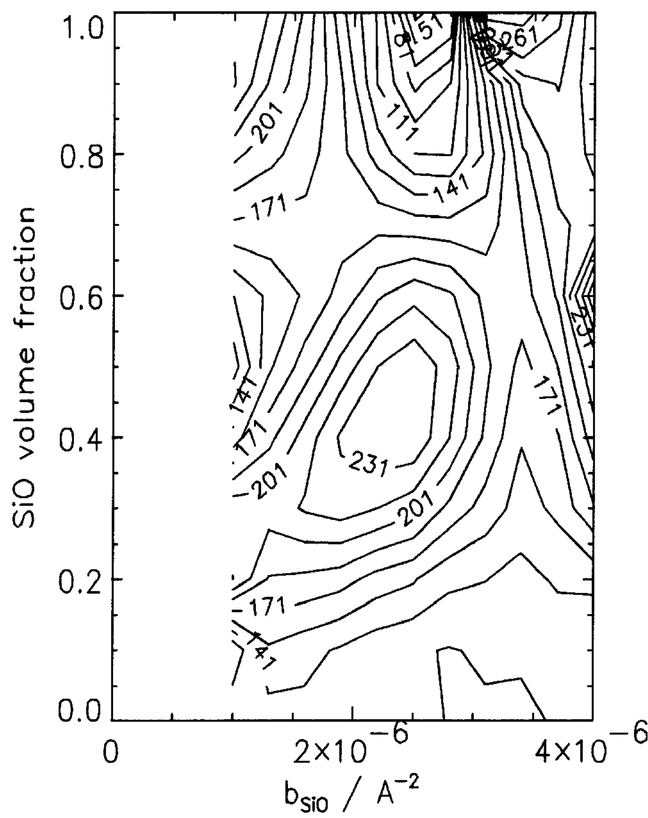

Figure 10. Contour χ^2 plot to show minimum at ($2{\cdot}6 \times 10^{-6}$ Å^{-2}, 0·95) for SiO 30°.

should be noted that in the SiO 30° case, a single layer approximation was adopted to avoid the same solution being reproduced each time if the χ^2 routine was executed with one layer of fixed SLD and volume fraction leaving the others free to refine. In these situations, often the thickness of the fixed volume fraction layer tends to zero for unfavourable volume fractions/SLDs, whilst the others expand to accommodate the same original SLD profile. A single layer approximation to the SLD profile avoids this confusion.

The case was not quite so simple for the SiO 5°. Owing to the numerous layers required to fit the data, it was not so simple to decide which parameters should be left to refine during the global minimum search. It was finally decided that the best method of obtaining a meaningful insight into the solution space was to let the volume fraction of the large porous layer vary whilst fixing the volume fractions of the two previous layers at unity. In doing this, the hexane free layers could not then take up the role of the third when it itself was fixed at an unfavourable SLD/volume fraction.

From the χ^2 plot it can be seen that although a global minimum was found at a SiO volume fraction equal to 0·65 and corresponding SLD of $2{\cdot}0 \times 10^{-6}$ Å^{-2}, the definition of the solution was not quite so marked as in

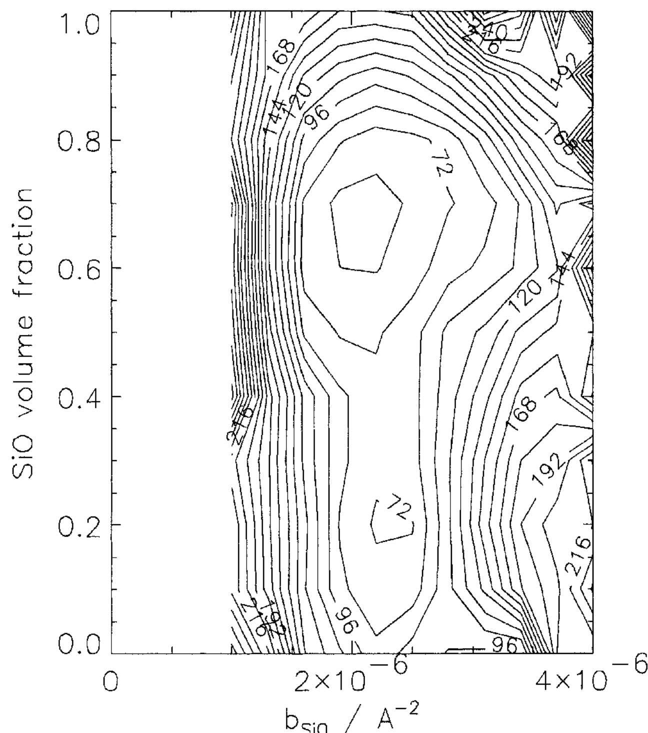

Figure 11. Contour χ^2 plot to show minimum at ($2{\cdot}1 \times 10^{-6}$ Å^{-2}, 0·67) for SiO 5°.

Downloaded At: 20:19 25 January 2011

the previous two cases. In fact a whole streak of solution space situated between volume fractions of 0·1 to 0·8 and at a SiO SLD of $2{\cdot}0 \times 10^{-6}$ Å^{-2} produced a χ^2 value not significantly different from the original solution. Owing to this poor definition of the SiO volume fraction in the χ^2 plots, we can only conclude that the SiO is porous with a volume fraction most probably in the region of 60–70% (30–40% hexane). Without data containing more characteristic features, it is difficult to determine accurately the precise nature of the volume fraction profile of hexane in SiO 5°.

6. Conclusions

In this study of SiO 5°, SiO 30° and the polyimide PI-32 alignment layers, a correlation was found between alignment layer porosity/surface roughness and induced pre-tilt. Rubbed polyimide and SiO 30° alignment layers were found to be smooth, uniform and impervious to hexane, whilst the SiO 5° was irregular in composition, porous and extremely rough. Similar conclusions on the porosity of such layers have been obtained from surface plasmon resonance results [32]. Of interest is the similarity of the polyimide and SiO 30° characteristics and their contrast to the SiO 5° which has the same chemical composition as the SiO 30° layer. The implication of these observations on the mechanisms for liquid crystal alignment is that both polyimide and SiO 30° rely on some sort of interaction mechanism rather than one induced by the surface topography. In contrast, the alignment of liquid crystals by SiO 5° probably originates from an interaction between the mesogens and rough SiO surface. A proposed mechanism for this is the 'order electric' model [33] where the interaction of a nematic with a rough surface reduces the order parameter and induces order electric anchoring of the director at an oblique angle. A layer of isotropic material near such a rough surface has recently been deduced from surface plasmon resonance results. However it seems likely that the very definite tilt of the columns will also have a significant influence on the alignment mechanism.

It remains to be seen how different liquid crystal phases (rather than a simple liquid) penetrate these alignment layers. However, we believe that the system studied in this work provided a valuable insight into the structure of the alignment layer and possible mechanisms of liquid crystal alignment by rubbed polyimide and obliquely evaporated silicon monoxide.

Downloaded At: 20:19 25 January 2011

References

[1] Myrvold, B. O., 1989, *Liq. Crys.*, **4,** 637.

[2] Kaho, S., Masumi, T., Tahata, S., Mizunuma, M., and Miyake, S., 1991, *Mol. Cryst. liq. Cryst.*, **199,** 87.

[3] Berreman, D. W., 1973, *Mol. Cryst. liq. Cryst.*, **23,** 215.

[4] Zhu, Y.-M., Wang, L., Lu, Z.-H., and Wei, Y., 1994, *Appl. Phys. Lett.*, **65,** 49.

[5] Pidduck, A. J., Bryan-Brown, G. P., Haslam, S. D., Bannister, R., Kitely, I., McMaster, T. J., and Boogaard, L., 1996, *J. Vac. Sci. Technol. A*, **14,** 1723.

[6] Takashi, I., Nakanishi, K., Nishikawa, M., Yokoyama, Y., and Takeuchi, Y., 1995, *Polym. J.*, **27,** 240.

[7] Toney, M. F., Russell, T. P., Logan, J. A., Kikuchi, H., Sands, J. M., and Kumar, S. K., 1995, *Nature*, **374,** 709.

[8] Ishihara, S., Hirofumi, W., Nakazima, K., and Matsuo, Y., 1989, *Liq. Cryst.*, **4,** 669.

[9] Geary, J. M., Goodby, J. W., Kmetz, A. R., and Patel, J. S., 1987, *J. appl. Phys.*, **62,** 4100.

[10] Barbero, G., Dozov, I., Palierne, J. F., and Durand, G., 1986, *Phys. Rev. Lett.*, **56,** 2056.

[11] Uchida, T., Ohgawara, M., and Wada, M., 1980, *Jpn. J. appl. Phys.*, **19,** 2127.

[12] Matsui, E., Nito, K., and Yasuda, A., 1993, *Ferroelectrics*, **149,** 97.

[13] Tarabia, M., Cohen, G., Davidov, D., and Escher, C., 1993, *Ferroelectrics*, **149,** 35.

[14] Jones, J. C., Towler, M. J., and Hughes, J. R., 1993, *Displays*, **14,** 86.

[15] Barmentlo, M., Hollering, R. W., and van Aerle, N. A. J. M., 1992, *Phys. Rev. A*, **46,** R4490.

[16] Als-Nielsen, J., 1985, *Z. Phys.*, **64,** 411.

[17] Hecht, E., 1987, *Optics*, 2nd edn (Addison-Wesley).

[18] Henderson, J. A., Richards, R. W., Penfold, J., Thomas, R. K., and Lu, J. R., 1993, *Macromolecules*, **26,** 4591.

[19] Penfold, J., 1991, *Neutron, X-ray and Light Scattering*, edited by P. Lindner and T. Zemb (Elsevier Science).

[20] Heavens, O. S., 1955, *Optical Properties of Thin Films* (London: Butterworth).

[21] Pidduck, A. J., Bryan-Brown, G. P., Haslam, S. D., and Bannister, R., 1996, *Liq. Cryst.*, **21,** 759.

[22] Penfold, J., Ward, R. C., and Williams, W. G., 1987, *J. Phys. E.*, **20,** 1411.

[23] Bucknall, D. G., Penfold, J., Webster, J. R. P., Zarbakhsh, A., Richardson, R. M., Rennie, A., Higgins, J. S., Jones, R. A. L., Fletcher, P., Thomas, R. K., Roser, S., and Dickinson, E., 1995, *SURF—A Second Generation Neutron Reflectometer*, ICANS XIII Conference Proceedings, 1995, PSI Proc. 95-02.

[24] Sinha, S. K., Sirota, E. B., Garott, S., and Stanley, H. B., 1988, *Phys. Rev. B.*, **38,** 2797.

[25] Névot, L., and Crocé, 1989, *Phys. Appl.*, **15,** 761.

[26] Haslam, S. D., and Pidduck, A. J., unpublished results.

[27] Kim, Y. B., Olin, H., Park, S. Y., Choi, J. W., Komitov, L., Matuszczyk, M., and Lagerwall, S. T., 1995, *Appl. Phys. Lett.*, **66,** 2218.

[28] Barberi, R., Giocondo, M., Sayko, G. V., and Zvedin, A. K., 1994, *J. Phys. Condens. Matter*, **4,** A27.

[29] Jerome, B., Pieranski, P., and Boix, M., 1988, *Europhys. Lett.*, **5,** 693.

[30] Phillips, P. L., 1995, unpublished results.

[31] Phillips, P. L., Richardson, R. M., and Cubitt, R., 1996, *J. Appl. Crystallog.*, Proceedings of the Xth International Conference on Small Angle Scattering (in press).

[32] Papánek, J., and Martinot-Lagarde, Ph., 1996, *J. Phys. II Fr.*, 205–214.

[33] Monkade, M., Boix, M., and Durand, G., 1988, *Europhys. Lett.*, 697.